Time delay in molecular photoionization

P Hockett[1], E Frumker[2], D M Villeneuve[3] and P B Corkum[3]

[1] National Research Council of Canada, 100 Sussex Drive, Ottawa, K1A 0R6, Canada
[2] Department of Physics, Ben-Gurion University of the Negev, Beer-Sheva 84105, Israel
[3] Joint Attosecond Science Laboratory, National Research Council of Canada and University of Ottawa, 100 Sussex Drive, Ottawa, K1A 0R6, Canada

E-mail: paul.hockett@nrc.ca

Abstract
Time-delays in the photoionization of molecules are investigated. As compared to atomic ionization, the time-delays expected from molecular ionization present a much richer phenomenon, with a strong spatial dependence due to the anisotropic nature of the molecular scattering potential. We investigate this from a scattering theory perspective, and make use of molecular photoionization calculations to examine this effect in representative homonuclear and hetronuclear diatomic molecules, nitrogen and carbon monoxide. We present energy and angle-resolved maps of the Wigner delay time for single-photon valence ionization, and discuss the possibilities for experimental measurements.

Keywords: attosecond, photoionization, Wigner delay, angle-resolved, molecular

(Some figures may appear in colour only in the online journal)

1. Introduction

The photoelectric effect—the emission of an electron from matter illuminated by light—is one of the most fundamental phenomena in nature, which historically led to Einstein's ground-breaking proposal of the quantization of light [1] and played a key role in the development of quantum mechanics. In the early works, the electron emission was tacitly assumed to be instantaneous, following the absorption of the excitation photon. However, more than half a century ago, it was predicted theoretically that there should be a time delay in the photoelectron emission process [2, 3], but it was only with the recent advances in attosecond science that direct measurements of electron dynamics with attosecond time resolution [4] required for the experimental validation of this prediction could be realized. Time resolved measurements of electron dynamics were reported [5–8] and the delay of photoemission was observed in condensed matter [9] and atoms [10, 11] in the single photon weak-field regime. However, no measurements of photoemission time delays from molecular targets have been reported as yet. Here we discuss theoretical results of angle and energy resolved time delays in the photoionization of molecules, and the prospects for direct measurement of this rich attosecond phenomena.

In scattering theory the phase of the transmitted wave is a direct consequence of the interaction of the incident wave with the scattering potential. Consequently, the scattering phase can be associated with an advance or retardation of the transmitted wave caused by its interaction with the scattering potential $V(r, \theta, \phi)$, as measured in the asymptotic limit. This phase-shift is always relative to the $V = 0$ case. A repulsive potential will lead to a negative phase, signifying an advance of the transmitted wave, while an attractive potential will lead to a positive phase, signifying a retardation (or trapping) of the transmitted wave. These results are most simply derived in a stationary state (energy-domain) picture of scattering, but a wavepacket (time-domain) treatment yields the same essential features [12]. Hence, in a time-domain picture of photoionization, the scattering phase-shift and associated time delay can be viewed as a group delay of the outgoing photoelectron wavepacket, born at a time t_0 within the ionizing laser pulse. In this case, the advanced wavepacket appears sooner than it would for the $V = 0$ case, while the retarded wavepacket appears later than it would for $V = 0$. This temporal response to the phase-shift is given by the Wigner delay, τ_w, which is determined by the energy-derivative of the scattering phase [2, 3].

While the concept of the Wigner delay is well established [2, 3], interest has recently been rekindled due to the

experimental accessibility of the attosecond time domain. Experiments using attosecond XUV pulse trains or isolated attosecond XUV pulses have been able to measure the relative group delay of electron wavepackets from atomic emission following single-photon absorption from a weak XUV field, with the measurements additionally requiring the interaction of the electron wavepacket with an IR field [10, 11]. The related possibility of determining an absolute photoionization time t_0 was discussed in this context [10], and has also been explored in the strong-field regime via tunnel ionization with 'attoclock' measurements [7], which employ pulses with rapidly changing instantaneous polarization vector (e.g. circularly polarized light) to obtain high temporal resolution via angular streaking of the photoelectron wavepackets.

In concert with these new experimental capabilities, numerous theoretical and computational studies have been performed. These can broadly be categorised as methodologies based on (a) canonical scattering theory [13–16], or (b) fully-numerical approaches based on the time-dependent Schrodinger equation [17, 18]. In most cases Wigner delays from the ionization of atomic targets have been of interest, and the angle-dependence of the process has not been investigated; notable exceptions to this trend are the recent work of Wtzel *et al* [19], who investigated the angle-dependence of the Wigner delay in detail for ionization of neon and argon, and studies of H_2—the simplest molecular scatterer—from Serov *et al* [20], which includes some consideration of the angle-dependence[5]. Conceptually, these methods are of course similar—one is seeking to solve equations that determine the continuum electron wavefunctions, and obtain scattering phase-shifts.

The main distinction that can be drawn between these approaches is the generality of the method and the information content of the results. A fully numerical treatment is, in principle, completely general, although in practice may be limited by computational cost; nonetheless, if performed carefully, the 'correct' final state wavefunction should be found for any given scattering system. A particular strength of time-dependent numerical methods is the ability to treat rapidly-varying scattering potentials, therefore allowing the effects of strong laser-fields to be incorporated into calculations. Such calculations have been employed in order to model experiments incorporating strong fields [21–23], which cannot be treated adequately by a time-independent approach. More traditional scattering theory approaches are usually time-independent and most suited to the weak field regime, hence are appropriate for the consideration of the intrinsic Wigner delay of the scattering system. Such approaches often use a *partial-wave* formalism, which allows separation into 'geometric' and 'dynamical' parts. In this case much progress can be made analytically, and a deep physical insight into the

characteristics of the scattering can be gained (see, for example, [24]). However, to obtain a complete solution to a complex scattering problem numerical methods are still ultimately needed for the dynamical part, and a specific formalism for the scattering system of interest is usually constructed in order to yield tractable equations (see, for example, [13, 20]); solving molecular scattering problems is therefore non-trivial for even the simplest cases. This problem can, however, be addressed via the use of variational techniques to solve the numerical part of the problem [25], allowing for a methodology which retains the full physical insights of scattering theory and the generality of fully-numerical approaches, but at a significantly lower computational cost.

In this work, we investigate Wigner delays from molecular ionization based on this general approach. We explore the details of the time delay in the valence ionization of N_2 and CO, based on calculations for single-photon ionization processes. The influence of the XUV field on both the bound states and the continuum electron are neglected, hence the results obtained correspond to the intrinsic Wigner delays of the photoemission process in the weak-field limit. We do not include any additional continuum-continuum delays, which can be a significant contribution to the total observed delay in the case of the XUV-IR measurements discussed above, but are dependent on the experimental technique [15] and not a fundamental property of the ionizing system. In this limit, the effect of the molecular potential on the energy and angle-resolved Wigner delay can be explored. This fundamental exploration forms the main thrust of the manuscript. Although the details are specific to valence ionization of N_2 and CO, the results may be considered as prototypical for molecular ionization. As detailed below (section 3), we make use of ePolyScat [26–28], a well-developed suite of codes from the scattering community, to solve the numerical integrals for arbitrary molecular potentials, thus our methodology is completely general and can be readily applied to polyatomic molecules. We finish by discussing some attosecond metrology concepts which could provide deeper experimental insight into ionization time delays in an angle and energy resolved manner.

2. Wigner time delay

As discussed by Wigner [2], Smith [3] and, more recently, in some depth by various authors [29–31], the phase of the scattering wavefunction can be associated with a time delay of the outgoing wavepacket, Ψ_g. In a partial-wave decomposition, Ψ_g is expressed as a coherent sum over partial-waves, $\Psi_g = \sum_{lm} \psi_{lm}$. Here each component is defined by the quantum numbers (l, m), the electronic orbital angular momentum and its projection onto a given quantization axis respectively, and each (l, m) pair defines a partial-wave scattering channel.

[5] For a fuller discussion of these extant techniques and theoretical treatments, the reader is referred to recent literature from Dahlstrm and co-workers, in particular [15, 30]; also of particular relevance to this study is the recent work of Wtzel *et al* [19], as mentioned in the main text, and related work on argon from Dahlstrm and Lindroth [16], which also includes discussion of the angle-dependence.

The time delay in a given channel is simply the derivative of the phase with respect to energy:

$$\tau_{\mathrm{w}}(\epsilon) = \hbar \frac{\mathrm{d}\eta_{lm}(\epsilon)}{\mathrm{d}\epsilon}, \tag{1}$$

where $\eta_{lm} = \sigma_l + \delta_{lm}$ is the total scattering phase, comprised of a central-potential (Coulombic) contribution σ_l and non-central (non-Coulombic) contribution δ_{lm}. For a Coulomb potential τ_{w} can be obtained directly from σ_l, which can be determined analytically, but in the general (non-Coulombic) case the total phase η_{lm} must be determined numerically. (It is of note that this definition of the Wigner delay does not include the full r-dependence of the phase of the outgoing wavefunction, which is divergent for an infinite-range Coulomb potential—a more general definition incorporating the total phase is given below. For further discussion of this point, the reader is referred to [31], for the specific case of Wigner delays, and [32] for a more general discussion.)

Similarly, the group delay of the outgoing electron wavepacket can be defined as the (coherent) sum over all constituent channels:

$$\tau_{\mathrm{w}}^{\mathrm{g}}(\epsilon) = \hbar \frac{\mathrm{d}\eta_{\mathrm{g}}(\epsilon)}{\mathrm{d}\epsilon}. \tag{2}$$

Here η_{g} represents the total (group) scattering phase, determined from Ψ_{g}, hence from the coherent summation over the partial-wave channels.

The significance of τ_{w} is as a time-domain manifestation of the scattering phase η_{lm}. Both contain the same information, namely the effect of the interaction potential on the outgoing wave, expressed as either a phase or delay. As noted above, this definition means that τ_{w} does not directly express the 'ionization time' in terms of the timescale of the interaction of the system with a photon (or perturbing electric field), rather it describes the time taken for the outgoing wavepacket to leave the influence of the potential, as defined by an effective range beyond which free-particle behaviour is assumed, and expressed relative to the time taken for a free particle with the same asymptotic velocity. In this sense a true reference time, t_0, is only specified to be within the duration of the ionizing radiation field[6].

In atomic ionization, the relatively simple nature of the scattering potential results in a continuum wavepacket with little spatial structure, which can often be described by just two partial-wave channels. In molecular ionization, the anisotropic nature of the potential means that many more partial-waves are required to describe the photoelectron wavepacket, and significant spatial and energy structure is expected. In essence, the angular structure of the photoelectron

wavepacket is the result of the angular interferences between the partial-waves at a given energy, while the difference in the dependence of the phase-shift of any given l-wave on the photoelectron kinetic energy results in the strong energy-dependence of the photoionization cross-section and τ_{w}.

The consequence of the angular dependence is, naturally, different τ_{w} as a function of angle, most clearly defined in the ionizing or molecular frame. We can rewrite equation (2) for this more general case:

$$\tau_{\mathrm{w}}(k, \theta, \phi) = \hbar \frac{\mathrm{d}\arg(\psi_{lm}^*(k, \theta, \phi))}{\mathrm{d}\epsilon}. \tag{3}$$

In this case we explicitly write τ_{w} as a function of the partial-waves $\psi_{lm}(k, \theta, \phi)$, labelled as a function of photoelectron momentum k, and polar and azimuthal angles (θ, ϕ) relative to the molecular axis. These wavefunctions contain both the scattering phase $\eta_{lm}(k)$ plus an angular contribution $Y_{lm}(\theta, \phi)$. The complex conjugate is required here because the scattering phase appears as $\mathrm{e}^{-\mathrm{i}\eta_{lm}}$ in ψ_{lm} (for a discussion of continuum wavefunctions in photoionzation, see [32]). As before, this equation expresses τ_{w} for each partial wave channel, and the group delay results from the sum over all (l, m) terms:

$$\tau_{\mathrm{w}}^{\mathrm{g}}(k, \theta, \phi) = \hbar \frac{\mathrm{d}\arg\left(\sum_{l,m} \psi_{lm}^*(k, \theta, \phi)\right)}{\mathrm{d}\epsilon}. \tag{4}$$

In this work we examine the form of the energy and angle-resolved group delay for two specific benchmark cases, valence ionization of the diatomic molecules N_2 and CO, and consider how the delay responds to the details of the molecular potential and the resulting continuum wavefunction.

3. Group delay in the molecular frame

3.1. Numerical details

Ionization matrix elements, which include the full scattering phase, were calculated using the ePolyScat suite of codes, distributed by R R Lucchese (for further details see [26–28]). These calculations take input from standard electronic structure codes (Gamess, Gaussian etc.) to define the initial state of the system. Ionization is treated as a one-electron process, leading to an $N - 1$ electron system and a free electron (hence there are no multi-electron effects in the sense of core relaxation, polarization etc.). The continuum wavefunction is solved numerically in the $N - 1$ electron potential, via a Schwinger variational procedure [25], and ionization matrix elements (within the dipole approximation) are calculated as the spatial overlap of this wavefunction and the initial orbital wavefunction, for a given polarization of the light and at a single photoelectron energy. This approach has been shown to work well in the weak field regime [25], and also for calculation of recombination matrix elements in HHG [33] although, in general, it is not an appropriate technique for the strong field regime as the laser field is not included in the scattering calculations.

---

[6] While this is rigorously true for any single ionization event, it is possible to obtain a time-resolution in practice that is better than the pulse duration via the use of statistical sampling or, potentially, through multi-photon ionization processes. For an ionizing pulse longer than τ_{w} interferometric measurements which are sensitive to the scattering phase may be used as an energy-domain proxy for direct measurement of τ_{w}. Since τ_{w} is typically on the order of tens of attoseconds, in most cases this absolute delay in photoemission is not measured, but rather an interferometric measurement sensitive to the relative delay between interfering wavepackets. For a more detailed discussion, see [30].
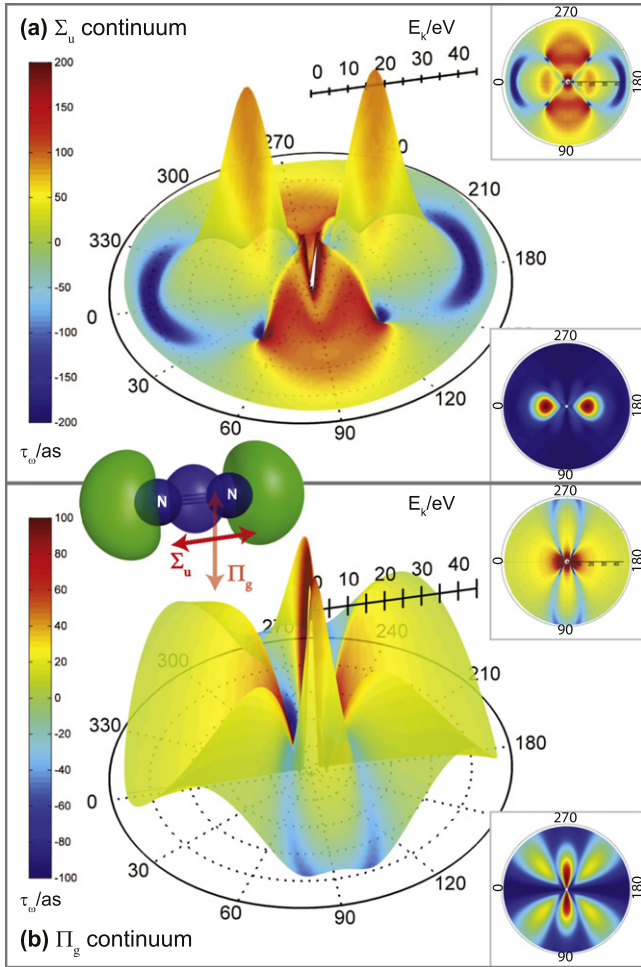
J. Phys. B: At. Mol. Opt. Phys. **49** (2016) 095602

P Hockett *et al*

Figure 1. Group delays for ionization of N_2 ($3\sigma_g \rightarrow k\sigma_u$, $k\pi_g$). (a) Σ_u continuum, (b) Π_g continuum. The main plots show polar surfaces, as a function of photoelectron kinetic energy and angle, with the topography defined by the photoionization cross section and colour-map by the Wigner delay τ_w^g; insets show the same data as 2D polar colour-maps, upper plot for τ_w^g (same scale as main colour-map) and lower plot for photoionization cross-sections (arb. units).

Figure 2. Group delays for CO ($5\sigma \rightarrow k\sigma$, $k\pi$). (a) Σ continuum, (b) Π continuum. The main plots show polar surfaces, as a function of photoelectron kinetic energy and angle, with the topography defined by the photoionization cross section and colour-map by the Wigner delay τ_w^g; insets show the same data as 2D polar colour-maps, upper plot for τ_w^g (same scale as main colour-map) and lower plot for photoionization cross-sections (arb. units).

In this work, calculations were based on equilibrium geometries and electronic structure from Gamess calculations (run at a relatively low, but appropriate, level of theory: RHF/MP2/6-311G) [34], with equilibrium bond lengths found to be 1.07 Å (N_2) and 1.12 Å (CO). Continuum wavefunctions and dipole matrix elements were computed with ePolyScat, for the highest-lying σ-orbitals in both cases, for linearly polarized ionizing radiation in both parallel and perpendicular geometries, and for photoelectron energies from 1 to 45 eV. The phase information from the raw matrix elements, expressed in terms of angular momentum channels, provides the full scattering phase-shift, and application of equation (3) provides τ_w for each channel. Similarly, equation (4) provides the group, or photoelectron wavepacket, delay. In the calculations, radial integrals are evaluated for $r_{max} = 10$ Å, defining an effective range to the interaction at which the total
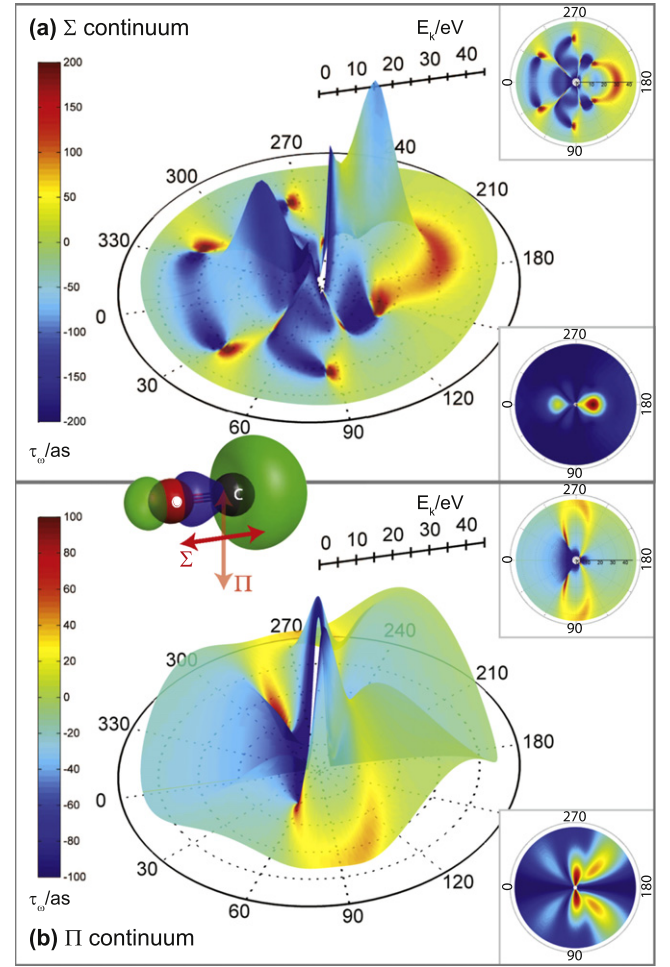
phase (hence delay) is defined. By calculating the photoionization matrix elements for a range of photoelectron energies, the energy dependence of the process can be mapped out, and the complete dependence of the Wigner delay $\tau_w(k, \theta, \phi)$ obtained.

In the following, we present and discuss these results for the general reader. Supplementary materials, including additional technical details of the results, e.g. channel-resolved dipole matrix elements, which may be of interest to some readers, are available online via Figshare at http://dx.doi.org/10.6084/m9.figshare.2007486.

3.2. Results

The results for the group (channel-integrated) Wigner delay, $\tau_w^g(k, \theta, \phi)$, for nitrogen and carbon monoxide are shown in figures 1 and 2, and represent the main results of this work. In the standard notation of *ionizing orbital* → *continuum wave* the one-electron ionization channels are given as
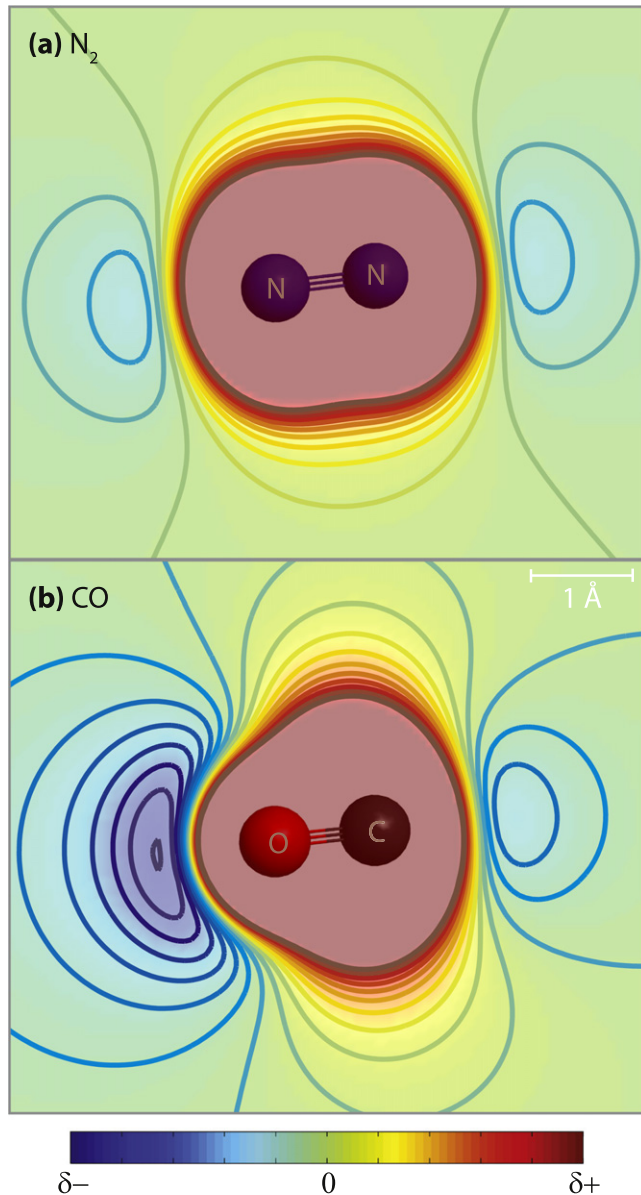
Figure 3. Molecular electrostatic potentials. (a) N_2, (b) CO. Contours show the long-range part of the molecular potential, with the colour scale indicating slightly positive ($\delta+$) and slightly negative ($\delta-$) regions.

$3\sigma_g \rightarrow k\sigma_u$, $k\pi_g$ for N_2 and $5\sigma \rightarrow k\sigma$, $k\pi$ for CO [25]. In the following discussion these cases are denoted by the overall N-electron symmetry ($\Gamma_{ion} \bigotimes \Gamma_{electron}$) and species, e.g. $N_2(\Sigma_u)$, CO(Π) etc.

Due to the cylindrically symmetric nature of these molecules, the ϕ-coordinate is redundant in these cases, and we can show the complete results as polar surface plots, as a function of energy and angle θ (relative to the molecular axis), without any loss of information. In these plots the surface topography follows the magnitude of the dipole matrix element (proportional to the square-root of the photoionization cross-section), while the colour-map shows the energy and angle-resolved Wigner time. As an alternative presentation of the results, which may be clearer in print, the insets show the same data as polar colour-maps. The Σ and Π continua shown

correspond to parallel or perpendicular laser polarization in the molecular frame respectively. The difference in peak magnitude between the continua is not shown in the figures, which are independently normalized to emphasize the angular structure, but it is of note that the Σ continua dominate in both cases, with the peak magnitude ratios of $\sim$2.4:1 for $N_2(\Sigma_u):N_2(\Pi_g)$, and $\sim$5.3:1 for CO(Σ):CO(Π). The molecular structure and ionizing orbital are also shown for reference, and the laser polarizations correlated with the different photoionization continua accessed are indicated.

These results present a complete, but complicated, picture of the molecular photoionization event, and the associated Wigner delay for the outgoing photoelectron wavepacket. It is immediately apparent that there is a significant amount of structure observed, both as a function of energy and angle, with τ_w^g values ranging from -200 to $+200$ as.

In both cases, the ionizing orbital is the valence σ-bonding orbital, with lobes oriented along the molecular axis. The choice of polarization of the ionizing radiation—either parallel or perpendicular to the molecular axis—defines the symmetry of the ionization continuum accessed, hence the symmetry of the continuum photoelectron wavefunction. For both N_2 and CO, this results in peaks in the cross-section along the molecular axis ($\theta = 0°$, $180°$) for the parallel case (figures 1(a) and 2(a)), and orthogonal to the molecular axis ($\theta = 90°$, $270°$) for the perpendicular case (figures 1(b) and 2(b)). Weaker additional lobes are also observed in all cases, but are most pronounced in the CO(Π) case, where they peak only around 20% lower than the perpendicular features. Furthermore, the lack of inversion symmetry in CO results in a significant difference in the cross-sections between the oxygen ($\theta = 0°$) and carbon ($\theta = 180°$) ends of the molecule, which is clear in both the Σ and Π continua, and again particularly pronounced in the additional lobes in the Π case, which dominate the cross-section around the carbon end of the molecule ($\theta = 140°$, $230°$).

4. Scattering dynamics

Physically, the peaks in the cross-section correspond to maxima in the dipole integrals which define the coupling between initial orbital and final continuum wavefunctions induced by ionizing radiation, with an angular dependence given by the partial-wave interferences. For $N_2(\Sigma_u)$ this peak is the well-known shape-resonance [25, 35, 36], corresponding to an enhancement of the $l = 3$ partial-wave, which can be considered as a trapping of this part of the outgoing wavepacket due to the form of the molecular potential energy surface. It is therefore not unexpected that the Wigner delay is also long in this region. Less expected are the lobes almost perpendicular to the molecular axis seen in figure 1(a), and associated long delays. This can be physically rationalized as a trapping of the outgoing wave in the bonding region (i.e. the nitrogen–nitrogen triple bond), resulting in a long Wigner delay. For $N_2(\Pi_g)$ the symmetry of the problem results in a nodal plane along the molecular axis, so there is much

reduced overlap between the main lobes of the ionizing orbital and the Π_g continuum, as compared to the Σ_u case. Here the cross-section looks akin to scattering through a slit, with a main feature and lower-intensity side lobes, and the cross-section peak is significantly reduced as compared to the Σ_u case, as discussed above. The dipole integral peaks much closer to 0 eV, and it is only in the low-energy region that large Wigner delays are predicted. For most of the energy and angular range the Wigner delay is close to zero, consistent with a classical diffractive picture of the ionization event, in which there is little trapping of the outgoing photoelectron wave.

In the case of CO the picture is quite different. Here the Wigner delays are predominantly negative, indicating a slight net repulsive effect from the molecular potential, and the results are highly asymmetric, consistent with the loss of inversion symmetry and the form of the ionizing orbital for a polar diatomic. The repulsive nature of the potential is most significant at the oxygen end of the molecule, where the extent of the ionizing orbital is much reduced relative to the carbon end. Chemically, the small extent of the orbital signifies the 'electronegativity' of the oxygen atom, which will tend to acquire a slight negative charge relative to the carbon atom. Based on chemical intuition, one might therefore expect to find a more repulsive potential than for the carbon end of the molecule, and this is borne out in the Wigner delay results. At higher energies, the Wigner delay at the carbon end becomes positive and large. This can be understood by consideration of the radial part of the continuum wavefunction: at higher energies the photoelectron wavelength becomes shorter, and the continuum function will become more penetrating relative to the core wavefunction. Consequently, the spatial overlap integral will incorporate more bound-state density closer to the core, which is effectively more strongly bound due to the slightly positive overall charge over the carbon atom, and will thus be delayed relative to bound-state density far from the core. At the oxygen end, the same change in overlap has the opposite effect, and continues to result in large negative Wigner delays due to the repulsive nature of the molecular potential over a large spatial region.

In order to visualize this behaviour, figure 3 shows the molecular electrostatic potentials $V(r, \theta)$ for both (neutral) molecules [37, 38]. In the figure, a cut through the cylindrically symmetric potentials are shown by both a colour-map and contours. The ranges plotted are chosen to highlight the long-range part of the potential which is most structured, and largely responsible for the complexity of the scattering problem. The short-range, highly positive, part of the potential, within which the majority of the bound electronic population resides, therefore appears structureless in these figures. Here it is clear that the negative, repulsive part of the potential is much more significant for CO than for N2, and most significant around the oxygen end of the molecule, thus leading to the most pronounced negative Wigner delays for wavepackets which experience this region. Conversely, the primarily attractive or neutral nature of the scattering potential
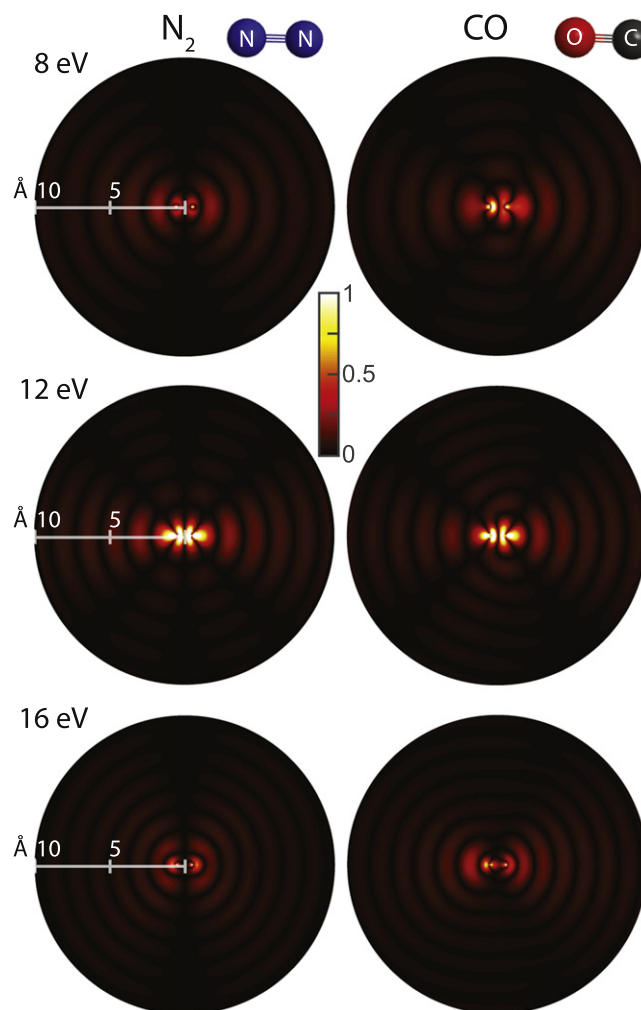
Figure 4. Continuum wavefunctions $|\psi(\theta, \phi)|$ for scattering from $N_2(\Sigma_u)$ and $CO(\Sigma)$ at $E = 8, 12, 16$ eV. Each plot is normalized to the peak of the wavefunction to highlight the spatial structure.

for N2, is responsible for the positive Wigner delays observed in the calculations.

Visualization of the scattering wavefunctions provides additional physical insight into the dynamics of the process. Figure 4 shows a selection of continuum wavefunctions at different photoelectron energies, chosen to represent the evolution of the scattering wavefunctions towards the peak in the cross-sections (shape-resonance), with symmetries concomitant with ionization parallel to the molecular frame ($N_2(\Sigma_u)$ and $CO(\Sigma)$). At the highest energy shown, the far-field wave-front (approximately established at length-scales as short as several Å [39]) shows little obvious angular structure correlated with the core, save for a basic two-centre scattering pattern. In contrast, at the two lower energies the angular structure is more complex, with the nodal planes more pronounced. This change in angular structure, for N2, is exactly the shape-resonance effect discussed above, with the observed continuum structure corresponding to the rise and fall of the $l = 3$ partial-wave component over this energy range, including a significant change in the magnitude of the wavefunction in the core region which has a strong effect on the overall ionization yield. For CO the

effect is slightly less clear, since the continuum structure is more complicated, but the general trend in complexity of the angular structure with energy is similar, and has been labelled by other authors as a shape resonance analogous to the N_2 case [25]. In all cases, the asymptotic phase-shift of the waves is approximately established at the length-scales shown ($r_{max} = 10$ Å), and phase differences can be observed in the plots. The lack of inversion symmetry in the far-field phases for CO is clear, with the phase shift between the carbon and oxygen ends of the molecule apparent in the intensity at the 10 Å cut-off.

Most generally, the complex structures observed for these two, relatively simple, diatomics might be regarded as indicative of molecular photoionization from valence orbitals, which invariably involves spatially diffuse, highly structured wavefunctions. The nature of the molecular potential, which is responsible for the shape of the bound-state orbitals, will similarly result in a continuum scattering wave which is highly sensitive to angle and energy. In this particular set of results, the effect of symmetry-breaking along the molecular axis is very clear, and in general larger molecules with lower symmetry may be expected to show similar, asymmetric, highly structured photoionization delays. The angular-sensitivity of the results points to the importance of angle-resolved measurement (or, equivalently, the loss of information inherent in angle-integrated measurements) for the investigation of molecular photoionization delays, and we consider this further in the following section.

5. Measurement

Recent measurements in atomic ionization using attosecond pulses have shown how τ_w can be measured in the time-domain. Ionization with attosecond XUV pulses, probed via streaking measurements [10], and side-band measurements [11] have been demonstrated. In both cases the effect of the IR probe field on the measurement is significant, and its effect on the photoelectron must be taken into account in order to model (or extract) and understand the measured delays. A series of theory papers have also discussed this issue (for example [15, 17, 21–23, 40]), most recently considering the angle-dependence of the time-delays in atomic ionization [16, 19], and left–right asymmetry in molecular ionization for CO [17].

In essence, the measurements work by mixing the electron wavepackets with the IR field, creating a spectrogram with modulations referenced to the carrier-envelope phase of the IR pulse. The streaking experiments used a strong IR field and FROG reconstruction of the resulting spectrogram in order to determine the delay between photoelectrons emitted from different initial states (and at different energies). The side-band measurement is based on single-photon absorption or emission in order to interfere photoelectrons from the same initial state, but created at different energies via different harmonic orders in the pump pulse train. This is effectively the RABBIT technique [41], but implemented to obtain

photoelectron scattering phases instead of optical phase information as per its original conception[7]. For example, [42] investigated the effect of ionization resonances on the phases obtain from RABBIT studies of molecular nitrogen. In essence, these types of measurement rely on phase differences between the interfering photoelectron wavepackets, so are sensitive to the difference in the group delays between different photoelectron energies, however they are angle-averaged over the photoelectron emission direction in the lab frame, and all partial-wave components. It is of particular note that the angle-resolved cross-section will weight the angle-integrated measurement towards the Wigner delays of the main angular features[8].

The scattering phases of individual partial waves, at a single energy, can be determined by measurements of photoelectron angular distributions. These are usually termed 'complete' photoionization experiments, and have been successfully demonstrated for a range of atomic and molecular ionization process (see [43, 44] for example, for more comprehensive reviews see [45, 46]), and most recently for multiphoton ionization with femto-second pulses, including electronic dynamics [47]. However, these measurements are typically not able to ascertain the phase structure with respect to energy, so can only determine η_{lm} for a given set of partial-waves with one of the waves serving as a reference. These types of measurement therefore provide detailed information on the angular part of the problem, including the phases of the contributing partial-waves, but do not directly provide a full mapping[9] of $\tau_w(k, \theta, \phi)$. The possibility of such experiments in the atto-second regime has also yet to be explored, although it is feasible that the broad energy bandwidths available would allow for phase structure as a function of energy to also be determined.

Ultimately, a combination of these techniques would be capable of measurements of the full $\tau_w^g(k, \theta, \phi)$. An angle-resolved RABBIT methodology would provide the energy and angular[10] dependence of τ_w^g, and measurements in this framework have very recently been investigated for atomic ionization [18, 48–50]. A detailed analysis of the photoelectron angular distributions—possibly from the same measurements, or more simply via direct ionization measurements—could provide complementary partial-wave information; the coupling of these two analyses could thus provide $\tau_w(k, \theta, \phi)$. The cleanest measurement strategy would also make use of molecular alignment, in order to choose only a single

---

[7] Interestingly, [41] notes that the electron scattering phase contribution to the RABBIT measurement can be 'easily taken into account' since it can be 'calculated from atomic theory with very good accuracy'. In the context of atomic ionization of simple species (H, He) this is reasonable, but does not hold for many electron systems, and certainly not for molecular scatterers.

[8] Angle-integrated Wigner delays corresponding to the exemplar cases presented herein can be found in the online supplementary materials at http://dx.doi.org/10.6084/m9.figshare.2007486.

[9] Although this is strictly correct, it is the case that careful analysis of PADs recorded at different energies, possibly combined with guidance from theory, can provide phase information as a function of energy. See, for example, [55]. With such an approach the full energy and angle-dependent $\tau_w(k, \theta, \phi)$ could be obtained.

[10] Interestingly, this proposition was already suggested in [41], but for the purpose of providing background free side-bands.

continuum symmetry. This would increase the complexity of the experiment, but allow for a decrease in the complexity of the analysis.

Very similar considerations have been explored in the context of high-harmonic generation (HHG). In particular, angle and energy resolved phase measurements of Br_2 were performed with the LAPIN technique [51]. In this technique, a two part measurement strategy (similar to that outlined above) is used in order to provide data which allows for reconstruction of the energy and angular dependence of the phase of the emitted high-harmonic radiation. In this case the measured emission phase includes contributions from strong-field ionization, propagation in the continuum and photo-recombination (this is the three-step model of HHG); the final step here is effectively equivalent to single-photon ionization. The experiments are based on two-source interferometry techniques: sensitivity to the angle-dependence of the phase is obtained in the case of two spatially distinct harmonic sources, both with Br_2 molecules, but with one source aligned and the other unaligned; sensitivity to the energy dependence of the phase is obtained in the case of two distinct species of emitter, with harmonics generated from a mixed gas containing Br_2 and a reference atom (Xe). The combination of the measurements, combined with a self-consistent phase-reconstruction procedure, provided angle and energy-dependent phase information. The reconstructed phases agreed reasonably well with theoretical results, which were based on ePolyScat calculations similar to those employed herein. Although a relatively involved procedure, the complete phase information obtained with the LAPIN technique will contain $\tau_w^g(k, \theta)$ from the recombination process, however other sources of delay will be present.

Another related study from the field of HHG is that of measurements on oriented CO, which was combined with a theoretical treatment (again within the standard three-step model) in order to understand the various phase contributions to the emitted harmonics [52]. In this case the prediction of even harmonics relied on both the difference in phase between the ends of the molecule, and the phase accrued during the tunnel ionization and propagation steps (also directionally dependent due to the shape of the molecular potential). Although these measurements are made in the frequency domain, the process can be understood in the time domain as attosecond bursts of harmonics occurring on each half-cycle of the driving laser field. The spectral interference of these bursts at the detector (hence integrated over the driving pulse duration and the generation volume) then determines the magnitude of the harmonics. Although this mechanism is responsible for all harmonic generation, in the CO experiments it is especially pertinent for understanding the effect of the asymmetry of the molecular potential, which results in different timings of the ionization and recollision leading to a phase difference which is mapped to the generated XUV bursts. In such measurements the global phase structure can be ascertained due to the bandwidth, or energy multiplexing, present. Although the spectral phase in this case was not measured directly, calculations based on a modified three-step model using time-dependent ionization and propagation calculations, combined with accurate recombination matrix elements (hence scattering phases) were able to recreate the intensity envelope of the harmonic spectrum and spectral phase differences between opposites end of the molecule. While not providing the full mapping of $\tau_w^g(k, \theta, \phi)$ discussed above, these types of measurements are very sensitive to phase differences in specific directions ($\theta = 0°$ versus $\theta = 180°$ in this case), and could therefore provide an interesting step towards full angle-resolved time-delay measurements, with the benefit of significantly reduced experimental complexity. One might consider that this frequency domain measurement of coherent attosecond processes is a technique sensitive to dynamics on the time-scale of τ_w, so could additionally be a sensitive probe of electronic dynamics.

A final point of note with regard to measurement of molecular versus atomic Wigner delays is the increased density of states in the molecular case. This suggests that the main difficulty in application of the measurement schemes discussed above, particularly to polyatomics, will likely be spectral congestion due to overlapping vibronic bands in the photoelectron spectrum. There is no general solution to this problem, since it is somewhat inherent to molecular ionization, but in many cases the issue may be side-stepped by judicious choice of spectral window(s) for RABBIT or similar types of measurement schemes, with the obvious cost of reducing the energy range which can be investigated. Alternatively, it may be possible to make use of this additional structure by, for instance, probing the effects on the Wigner delay of ionizing from different states, or via different intermediate states by making use of degenerate ionization processes of different photon orders. In both cases, degenerate photoelectrons will interfere (providing ensemble coherence is maintained, and the process is symmetry-allowed), and information on the Wigner delays associated with the different ionizing transitions will be contained in the measurement. Conceptually this is similar to the measurements of [10], which ascertained the difference in Wigner delay between photoelectron wavepackets originating from 2s and 2p ionizing states. However, in that case the measurement was made via streaking of energetically separated photoelectron bands, rather than via direct interference between the bands. Older frequency-domain work has investigated exactly the case of degenerate photoelectron band interferences suggested here, examples include coherent control and complete experiments [53, 54], and as a method sensitive to the Breit–Wigner phase shift of an intermediate bound-state [56]. However, in these cases only narrow energy ranges were considered, so these older works did not consider the energy-dependence of the photoionization phase and the associated Wigner delays.

6. Conclusions

Molecular ionization is a complex phenomenon, with the outgoing photoelectron wavepacket experiencing a highly anisotropic scattering potential. In the time-domain, this

J. Phys. B: At. Mol. Opt. Phys. **49** (2016) 095602

P Hockett *et al*

results in a highly-structured Wigner delay, as a function of energy and angle in the molecular frame. With the use of scattering calculations, the angle-dependent Wigner delay $\tau_w^g(k, \theta, \phi)$ was examined for two simple diatomics, and these results illustrate the magnitudes of the delays, and types of structures, which might generally be expected in molecular photoionization. The deep link between the Wigner delay and the photoionization matrix elements is also revealed in the correlation of energy-domain photoionization phenomena—in this case the shape resonance in N_2—with features in the Wigner delay. Physically, this correspondence arises from the mildly attractive and repulsive regions in the long-range part of the scattering potential, which largely determine the continuum photoelectron wavefunction at the energy ranges investigated. In a wavepacket picture, the same considerations are manifested as large changes in the photoelectron wave-packet dwell-times in these spatial regions, both as a function of energy and angle in the molecular frame. Finally, some concepts for the experimental measurement of angle-resolved Wigner delays were discussed, suggesting the possibility of experimental methodologies based on existing RABBIT measurements (and conceptually similar HHG studies) for the measurement of angle-resolved Wigner delays. While the outlook here is promising, given the highly-structured nature of the Wigner delay and molecular ionization continuum, such experiments will be very challenging.

Acknowledgments

References

[1] Einstein A 1905 Über die von der molekularkinetischen Theorie der Wärme geforderte Bewegung von in ruhenden Flüssigkeiten suspendierten Teilchen *Ann. Phys., Lpz.* **8** 549–60

[2] Wigner E 1955 Lower limit for the energy derivative of the scattering phase shift *Phys. Rev.* **98** 145–7

[3] Smith F 1960 Lifetime matrix in collision theory *Phys. Rev.* **118** 349–56

[4] Hentschel M, Kienberger R, Spielmann C, Reider G a, Milosevic N, Brabec T, Corkum P, Heinzmann U, Drescher M and Krausz F 2001 Attosecond metrology *Nature* **414** 509–13

[5] Uiberacker M *et al* 2007 Attosecond real-time observation of electron tunnelling in atoms *Nature* **446** 627–32

[6] Goulielmakis E *et al* 2010 Real-time observation of valence electron motion *Nature* **466** 739–43

[7] Eckle P, Pfeiffer A N, Cirelli C, Staudte A, Dörner R, Muller H G, Büttiker M and Keller U 2008 Attosecond ionization and tunneling delay time measurements in helium *Science* **322** 1525–9

[8] Schultze M *et al* 2014 Attosecond band-gap dynamics in silicon *Science* **346** 1348–52

[9] Cavalieri A L *et al* 2007 Attosecond spectroscopy in condensed matter *Nature* **449** 1029–32

[10] Schultze M *et al* 2010 Delay in photoemission *Science* **328** 1658–62

[11] Klünder K *et al* 2011 Probing single-photon ionization on the attosecond time scale *Phys. Rev. Lett.* **106** 143002

[12] Rodberg L S and Thaler R M 1967 *Introduction to the Quantum Theory of Scattering* (New York: Academic)

[13] Ivanov I A, Kheifets A S and Serov V V 2012 Attosecond time-delay spectroscopy of the hydrogen molecule *Phys. Rev. A* **86** 063422

[14] Kheifets a S 2013 Time delay in valence-shell photoionization of noble-gas atoms *Phys. Rev. A* **87** 063404

[15] Dahlström J M, Guénot D, Klünder K, Gisselbrecht M, Mauritsson J, L'Huillier A, Maquet A and Taïeb R 2013 Theory of attosecond delays in laser-assisted photoionization *Chem. Phys.* **414** 53–64

[16] Dahlström J M and Lindroth E 2014 Study of attosecond delays using perturbation diagrams and exterior complex scaling *J. Phys. B: At. Mol. Opt. Phys.* **47** 124012

[17] Chacon A, Lein M and Ruiz C 2014 Asymmetry of Wigner's time delay in a small molecule *Phys. Rev. A* **89** 053427

[18] Ivanov I A, Dahlström J M, Lindroth E and Kheifets A S 2015 On the angular dependence of the photoemission time delay in helium in preparation

[19] Wätzel J, Moskalenko a S, Pavlyukh Y and Berakdar J 2015 Angular resolved time delay in photoemission *J. Phys. B: At. Mol. Opt. Phys.* **48** 025602

[20] Serov V V, Derbov V L and Sergeeva T a 2013 Interpretation of time delay in the ionization of two-center systems *Phys. Rev. A* **87** 063414

[21] Baggesen J C and Madsen L B 2011 Atomic and molecular phases through attosecond streaking *Phys. Rev. A* **83** 021403

[22] Nagele S, Pazourek R, Feist J, Doblhoff-Dier K, Lemell C, Tokesi K and Burgdorfer J 2011 Time-resolved photoemission by attosecond streaking: extraction of time information *J. Phys. B: At. Mol. Opt. Phys.* **44** 081001

[23] Ning Q-C, Peng L-Y, Song S-N, Jiang W-C, Nagele S, Pazourek R, Burgdörfer J and Gong Q 2014 Attosecond streaking of Cohen–Fano interferences in the photoionization of H2+ *Phys. Rev. A* **90** 013423

[24] Dill D 1976 Fixed-molecule photoelectron angular distributions *J. Chem. Phys.* **65** 1130–3

[25] Lucchese R R, Takatsuka K and McKoy V 1986 Applications of the Schwinger variational principle to electron-molecule collisions and molecular photoionization *Phys. Rep.* **131** 147–221

[26] Gianturco F A, Lucchese R R and Sanna N 1994 Calculation of low-energy elastic cross sections for electron-CF_4 scattering *J. Chem. Phys.* **100** 6464–71

[27] Natalense A P P and Lucchese R R 1999 Cross section and asymmetry parameter calculation for sulfur 1s photoionization of sf[sub 6] *J. Chem. Phys.* **111** 5344–8

[28] Lucchese R R 2015 (www.chem.tamu.edu/rgroup/lucchese/)

[29] de Carvalho C A A and Nussenzveig H M 2002 Time delay *Phys. Rep.* **364** 83–174

[30] Dahlström J M, L'Huillier A and Maquet A 2012 Introduction to attosecond delays in photoionization *J. Phys. B: At. Mol. Opt. Phys.* **45** 183001

[31] Pazourek R, Nagele S and Burgdörfer J 2015 Attosecond chronoscopy of photoemission *Rev. Mod. Phys.* **87** 765–802

[32] Park H and Zare R N 1996 Molecular-orbital decomposition of the ionization continuum for a diatomic molecule by angle-

J. Phys. B: At. Mol. Opt. Phys. **49** (2016) 095602

P Hockett *et al*

and energy-resolved photoelectron spectroscopy: I. Formalism *J. Chem. Phys.* **104** 4554

[33] Le A-T, Lucchese R R, Tonzani S, Morishita T and Lin C D 2009 Quantitative rescattering theory for high-order harmonic generation from molecules *Phys. Rev.* **80** 013401

[34] Schmidt M W *et al* 1993 General atomic and molecular electronic structure system *J. Comput. Chem.* **14** 1347–63

[35] Shigemasa E, Adachi J and Oura M 1995 Angular distributions of 1s σ photoelectrons from fixed-in-space N_2 molecules *Phys. Rev. Lett.* **74** 359–62

[36] Hikosaka Y and Eland J H D 2000 Molecular-frame photoelectron angular distributions in inner-valence photoionization of N_2 *J. Phys. B: At. Mol. Opt. Phys.* **33** 3137–47

[37] Bode B M and Gordon M S 1998 Macmolplt: a graphical user interface for GAMESS *J. Mol. Graph. Modelling* **16** 133–8

[38] Bode B 2015 (http://brettbode.github.io/wxmacmolplt/)

[39] Knox W H, Alonso M and Wolf E 2010 Spatial coherence from ducks *Phys. Today* **63** 11–11

[40] Kheifets A S and Ivanov I A 2010 Delay in atomic photoionization *Phys. Rev. Lett.* **105** 233002

[41] Muller H G 2002 Reconstruction of attosecond harmonic beating by interference of two-photon transitions *Appl. Phys.* B **74** 17–21

[42] Haessler S *et al* 2009 Phase-resolved attosecond near-threshold photoionization of molecular nitrogen *Phys. Rev.* A **80** 011404

[43] Duncanson J, Strand M, Lindgård A and Berry R 1976 Angular distributions of electrons from resonant two-photon ionization of sodium *Phys. Rev. Lett.* **37** 987–90

[44] Reid K, Leahy D and Zare R 1992 Complete description of molecular photoionization from circular dichroism of rotationally resolved photoelectron angular distributions *Phys. Rev. Lett.* **68** 3527–30

[45] Reid K L 2003 Photoelectron angular distributions *Annu. Rev. Phys. Chem.* **54** 397–424

[46] Reid K L 2012 Photoelectron angular distributions: developments in applications to isolated molecular systems *Mol. Phys.* **110** 131–47

[47] Hockett P, Wollenhaupt M, Lux C and Baumert T 2014 Complete photoionization experiments via ultrafast coherent control with polarization multiplexing *Phys. Rev. Lett.* **112** 223001

[48] Laurent G, Cao W, Ben-Itzhak I and Cocke C L 2014 Attosecond control of electron emission from atoms *J. Phys.: Conf. Ser.* **488** 012008

[49] Heuser S, Sabbar M, Boge R, Lucchini M, Gallmann L, Cirelli C and Keller U 2015 Photoionization time delay dynamics in noble gas *CLEO: 2015* (Washington, DC: OSA) FTh4C.3

[50] Heuser S *et al* 2015 Time delay anisotropy in photoelectron emission from the isotropic ground state of helium (arXiv: 1503.08966)

[51] Bertrand J B, Wörner H J, Salières P, Villeneuve D M and Corkum P B 2013 Linked attosecond phase interferometry for molecular frame measurements *Nat. Phys.* **9** 174–8

[52] Frumker E *et al* 2012 Probing polar molecules with high harmonic spectroscopy *Phys. Rev. Lett.* **109** 233904

[53] Yin Y-Y, Chen C, Elliott D and Smith A 1992 Asymmetric photoelectron angular distributions from interfering photoionization processes *Phys. Rev. Lett.* **69** 2353–6

[54] Wang Z-M and Elliott D 2001 Determination of the phase difference between even and odd continuum wave functions in atoms through quantum interference measurements *Phys. Rev. Lett.* **87** 173001

[55] Yagishita A, Hosaka K and Adachi J-I 2005 Photoelectron angular distributions from fixed-in-space molecules *J. Electron Spectrosc. Relat. Phenom.* **142** 295–312

[56] Fiss J A, Khachatrian A, Truhins K, Zhu L, Gordon R and Seideman T 2000 Direct observation of a Breit-Wigner phase of a wave function *Phys. Rev. Lett.* **85** 2096–9